Russell J. Donnelly
Department of Physics
University of Oregon
Eugene, OR 97403
USA

Katepalli R. Sreenivasan
Department of Engineering
and Applied Sciences
Yale University
New Haven, CT 06520
USA

Library of Congress Cataloging-in-Publication Data
Donnelly, Russell J.
Flow at ultra-high Reynolds and Rayleigh numbers : a status report
/ Russell J. Donnelly, Katepalli R. Sreenivasan.
p. cm.
"The Brookhaven Workshop was sponsored by the National Science Foundation under grants DMR9614058 and DMR9529609"—p. iv.
Includes bibliographical references.
ISBN 0-387-98544-1 (alk. paper)
1. Liquid helium—Measurement—Congresses. 2. Reynolds number—Measurement—Congresses. 3. Rayleigh number—Measurement—Congresses. 4. Turbulence—Measurement—Congresses.
I. Sreenivasan, Katepalli R. II. Brookhaven Workshop. III. Title.
QC145.45.H4D65 1998
532'.05—dc21 98-7475

Printed on acid-free paper.

Production managed by Allan Abrams; manufacturing supervised by Joe Quatela.
Camera-ready copy supplied by the editors.
Printed and bound by Braun-Brumfield, Inc., Ann Arbor, MI.
Printed in the United States of America.

9 8 7 6 5 4 3 2 1

ISBN 0-387-98544-1 Springer-Verlag New York Berlin Heidelberg SPIN 10680200

Russell J. Donnelly Katepalli R. Sreenivasan
Editors

Flow at Ultra-High Reynolds and Rayleigh Numbers

A Status Report

With 239 Figures

Springer

13 *Matheson Unabridged Gas Data Handbook*, Matheson Gas Products, East Rutherford, NJ (1974).
14 L. Adler and C. Yaws, Solid State Tech. **18**(1), 35 (1975).
15 A. Oda, M. Uematsu, and K. Watanabe, Bulletin of the JSME **26**(219), 1590 (1983).
16 J. Hoogland, H. Van Den Berg, and N. Trappeniers, Physica A **134**, 169 (1985).
17 J. Kestin and N. Imaishi, Int. J. Thermophys. **6**, 107 (1985).
18 Allied-Signal Inc., SF_6 Thermodynamic Tables, Morristown, NJ (1991).
19 X. Z. Wu, Ph.D. thesis, University of Chicago, 1991 (unpublished).
20 A. Belmonte, A. Tilgner, and A. Libchaber, Phys. Rev. E **51**, 5681 (1995).
21 A. Tilgner, A. Belmonte, and A. Libchaber, Phys. Rev. E **47**, 2253 (1993).
22 T. Takeshita, T. Segawa, J. Glazier, and M. Sano, Phys. Rev. Lett. **76**, 1465 (1996).
23 R. Kraichnan, Phys. Fluids **5**, 1374 (1962).
24 E. S. C. Ching, preprint (1996).
25 A. Belmonte and A. Libchaber, Phys. Rev E **53**, 4893 (1996).
26 K. Sreenivasan, Proc. R. Soc. Lond. A **434**, 165 (1991).
27 I. Procaccia, E. S. C. Ching, P. Constantin, L. Kadanoff, A. Libchaber, and X. Z. Wu, Phys. Rev. A **44**, 8091 (1991).
28 J. Elder, J. Fluid. Mech. **23**, 77 (1965); *ibid* **23**, 99 (1965).
29 P. Bouruet-Aubertot, J. Sommeria, and C. Staquet, J. Fluid Mech. **285**, 265 (1995).
30 D. Benielli and J. Sommeria, Dyn. Atmos. Oceans **23**, 335 (1996).

High Rayleigh Number Turbulence of a Low Prandtl Number Fluid

T. Segawa, M. Sano, A. Naert, and J. A. Glazier†

Research Institute of Electrical Communication, Tohoku University, Sendai 980, Japan
† Department of Physics, University of Notre Dame, Notre Dame, IN

Abstract. We have studied the scaling properties of thermal turbulence in a low Prandtl number, Pr, fluid using liquid Hg ($Pr = 0.024$). The length scale of thermal and viscous boundary layers are analyzed from time series of movable thermistors near the boundary. It revealed that the thermal and viscous layer had crossed over the observed range of Rayleigh numbers ($10^6 < Ra < 10^8$). The frequency spectrum of the temperature fluctuations and the scaling of the cutoff frequency differed from those of He. The cascade range was smaller than expected. Characters of high Rayleigh number flow of a low Prandtl number fluid is discussed.

Introduction

Experimental studies on turbulence in thermal convection [1–5] have revealed a distinctive turbulent state called hard turbulence. The hard turbulence is characterized by: (1) The histogram of the temperature fluctuations at the center of the fluid has an exponential distribution. (2) Large scale bulk circulation coexists with turbulence. (3) The Nusselt number, Nu, the root mean square temperature fluctuation and the mean velocity U of the large scale flow all have power law dependence on the Rayleigh number, Ra, with scaling exponents different from classical theory [6]. (4) The temperature power spectrum decays as the power law with a slope close to -1.4 for $Ra < 10^{11}$ and two slopes for $Ra > 10^{11}$.

The scaling relations for the hard turbulence are summarized as follows,

$$Nu \sim Ra^{\gamma}, \tag{1}$$

$$\frac{UL}{k} \sim Ra^{\epsilon} \tag{2}$$

where L is the box size, κ is the thermal diffusivity, $\gamma = 0.285 \pm 0.004$ which is close to (2/7), and $\varepsilon = 0.485 \pm 0.005$. Theories explaining the scaling phenomena of hard turbulence, assume distinct boundary layers for the temperature and the velocity (viscous sublayer) fields, and that the entire temperature drop occurs within the viscous sublayer [2, 6, 7]. The thickness of the thermal boundary layer, λ_T, should scale as,

$$\frac{\lambda_T}{L} \sim \frac{1}{Nu} \sim Ra^{-\gamma}, \tag{3}$$

provided that the thermal boundary layer is purely diffusive ($\gamma = 2/7$ in the theory) [2, 7]. On the other hand, the thickness of the viscous boundary layer, λ_V, can be estimated by dimensional analysis as

$$\frac{\lambda_V}{L} \sim \frac{1}{Re} \sim Ra^{-\varepsilon}. \tag{4}$$

Relation between two exponents ($\varepsilon > \gamma$) implies that at high Rayleigh numbers, the viscous boundary layer may become thinner than the thermal boundary layer, violating the hypothesis that the thermal boundary layer is diffusion limited. Shraiman and Siggia [7] conjectured that hard turbulence is unstable if crossing occurs. Therefore hard turbulence may not be asymptotic for high Ra, but an intermediate. The relation, $Nu \sim Ra^{1/2}$ was predicted for the new state [6, 7, 8]. Recent direct measurements of boundary layers in pressurized SF_6 confirmed the dependence of λ_T and λ_V on Ra, and showed that the crossing should take place around $Ra \sim 10^{14}$, though these Ra were not obtained [10]. However, the Prandtl numbers of Belmonte et al.'s fluids were fairly high: $Pr = 0.7$ for Helium and compressed gas, $2 < Pr < 7$ for water. The lower the Prandtl number, the smaller the ratio of the boundary thicknesses, λ_V/λ_T, since the Reynolds number is higher. The critical Rayleigh number for this turbulence transition for liquid Hg ($Pr = 0.024$) should be $Ra \sim 10^5 - 10^7$ [7]. In this paper, we examine the statistical and scaling properties of low Prandtl number fluid (Hg) turbulence. We compare our results to hard turbulence in Helium and pressurized gas. The Reynolds number of the flow is about 10 times higher than for He at the same Ra. The power spectrum has a peculiar scaling, which results from the viscous boundary layer being as thin or thinner than the thermal boundary layer [9].

Experimental Setup

The experimental cell is a vertical cylinder 10 cm in height (L) and 10 cm in diameter (aspect ratio 1) as shown in Figure 1. The top and bottom plates are made of nickel plated copper 2 cm thick. The side wall cylinder is made of stainless steel 2 mm thick to match the thermal conductivity of Hg. The high thermal conductivity of mercury requires special heating and cooling. In the bottom plate, an insulated manganin wire heater (diameter 0.3 mm) is embedded with thermal conducting paste in a spiral groove of semicircular section, width 0.4 mm and spacing 0.6 mm.

The top plate forms the bottom of a large copper container with many copper fins embedded to promote good thermal exchange with the cooling water. Temperature controlled water enters the container through five inlets and exits from four outlets. The heater is supplied with constant power ranging from one watt to several hundred watts depending on the target Rayleigh number. The temperature of the cooling water is controlled in stages: first by a refrigerator and an electric heater, second by a 20 liter ballast tank, and finally by Peltier elements for precise control. The worst temperature stability occurs for maximal heating and is 1% of the total temperature difference, ΔT, between the top and bottom plates. The best stability occurs for minimal heating and is of the order of 10^{-4} K. To measure the local temperature fluctuations, we used five thermistors (Thermometric B07PA) whose size is 300 μm in diameter with insulation though the bare size is 200 μm. Their response time is sufficiently shorter than the flow's typical minimum time scale of 100–200 msec.

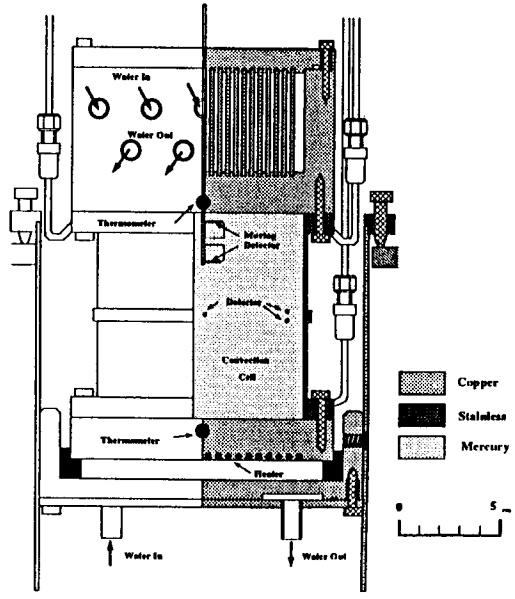

Figure 1. Convection cell.

As shown in Figure 2, one [A] is placed at the center of the cell at midheight, two are vertically aligned at 1 cm from the side wall, one at midheight [B1], and the other 2 mm above [B2] to measure the mean flow velocity. Two thermistors ([C] and [D]) are fixed on the fine stainless tube that is tied to micro-translational stage, controlled by a stepper motor, and can be moved vertically along the center line of the cylinder. Each thermistor constitutes one arm of an AC capacitance bridge whose output is fed to a lock-in amplifier (PAR 124A). The output signal is first digitized and stored in an HP digital spectrum analyzer (HP3563A) then analyzed by computer.

Experimental Results

The histogram of the temperature fluctuations is close to an exponential distribution for accessible Rayleigh numbers, $10^6 < Ra < 10^8$, verifying that the turbulence is well developed. Figure 2 shows the histogram of the temperature fluctuations at the center of the cell [A] for $Ra = 7.54 \times 10^7$.

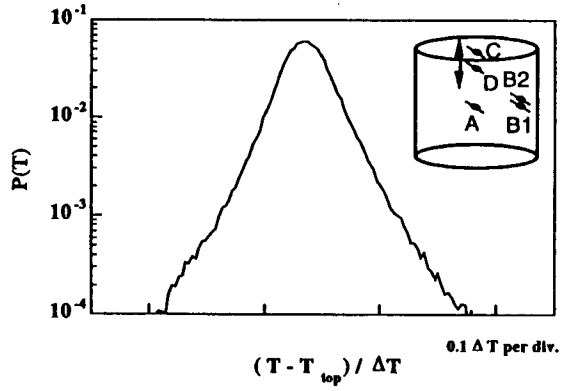

Figure 2. Nearly exponential histogram of temperature fluctuations measured by the center thermistor [A] at $Ra = 7.54 \times 10^7$. The inset shows a schematic drawing of the experimental cell with the positions of the thermistors.

Large scale circulation persists over the same range of Rayleigh numbers. We measured the mean flow velocity of the large scale circulation with two adjacent thermistors [B1, B2] near the side wall. We estimated the group velocity of temperature fluctuations passing through the two detectors from the phase delay of the cross spectrum of the two signals [3]. The mean flow velocity was about 2 cm/sec at Ra = 10^7. We obtained the Reynolds number at length L from the mean flow velocity V; $Re = VL/\nu$ in Figure 3. The large scale circulation causes the frequency peak of the temperature power spectrum, f_p [3]. Thus fp

also gives an estimate of the mean flow velocity, using relation $V \sim \pi L f_p$. We also plot the dimensionless parameter, $Re' + f_p * \pi L2/\nu$ in Figure 3. Direct and indirect measurements of mean flow velocity coincide. The scaling relation,

$$V/(\nu/L) \sim 6.24\, Ra^{0.47\pm0.02} \tag{5}$$

resembles hard turbulence in He but with a coefficient 20 times larger.

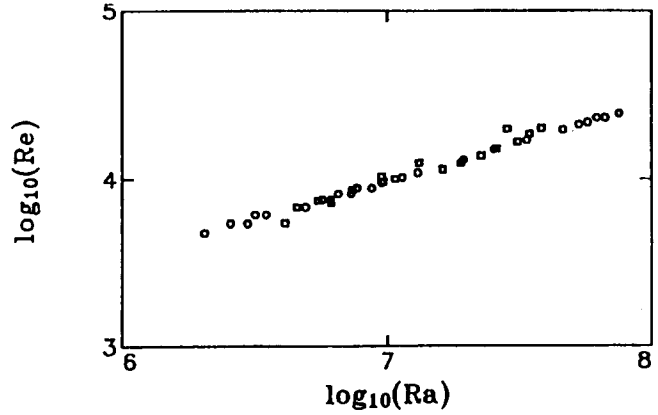

Figure 3. Scaling of the Reynolds number of the box, Re = VL/ν, measured by phase delay as a function of the Rayleigh number (rectangles). The mean flow velocity can be estimated from the frequency peak, f_p. The Reynolds number is compared to $\pi f_p L^2/\nu$ (circles). Both quantities fit the scaling $Re = 6.24 Ra^{0.46\pm0.02}$.

Reference [3] estimates that the transition to hard turbulence takes place when the Reynolds number of the box exceeds 10^3. As shown in Figure 3, Re is 10^4 at $Ra \sim 10^7$. Thus, even the lowest Ra (10^6) in our experiment is well within the hard turbulence regime. Extrapolating to lower Rayleigh number, suggests that hard turbulence in mercury starts around $Ra \sim 10^5$, not far from the onset of convection and chaos. Soft turbulence may occur over a narrow range or not exist in low Pr number fluids.

Figure 4 shows the power spectrum of temperature fluctuations at $Ra = 7.12 \times 10^7$. We fit the power spectrum with the function [4],

$$P(f) = \left(\frac{f}{f_0}\right)^{-\alpha} \exp\left(-\frac{f}{f_c}\right). \tag{6}$$

By fitting power spectra for Ra numbers ($10^7 < Ra < 10^8$), we obtain

$\alpha = 1.58 \pm 0.09$.

We determined the cutoff frequency, f_c, as a function of Ra. f_c scales as $f_c \sim Ra^{\beta}$, with $\beta = 0.4 \pm 0.05$. The exponent differs from that of He turbulence where $\beta = 0.78$ by the same method [14]. We can understand the exponent β in the He experiment as follows: the cutoff frequency depends on the smallest spatial structure (plume) of size Λ advected by the mean flow velocity, V. Thus $f_c \sim V/\Lambda$. Λ should be of the same order as the thickness of the thermal boundary layer, λ_T. Therefore $f_c \sim Ra^{\gamma+\varepsilon} \Rightarrow \gamma+\varepsilon \sim 0.77$ for He and SF_6 turbulence. However, the argument fails for mercury turbulence.

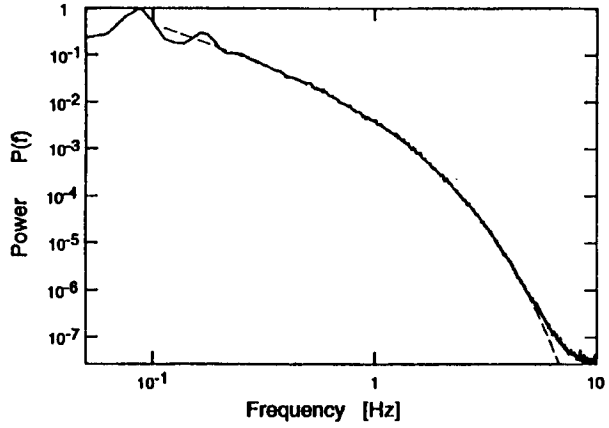

Figure 4. Frequency power spectrum of the side thermistor [B1] at $Ra = 7.12 \times 10^7$. The dotted line shows a fit to the function $P(f) = P_0(f/f_0)^{-\alpha} \exp -(f/f_c)$, $\alpha = 1.49$.

As shown in Figure 3, the frequency peak f_p scales as $f_p \sim Ra^{0.46\pm0.02}$. Comparing the scaling exponents for f_p and f_c in Hg, shows that the entropy cascade range [11, 12, 13] of the power spectrum unexpectedly shrinks with increasing Ra. This difference in scaling is the main puzzle of turbulent fluctuation of Hg.

We calculated the Nusselt number, Nu, from the power supplied to the bottom plate heater. The convection cell is surrounded by a thermal insulator and placed in a stainless steel outer jacket whose bottom temperature is set to the temperature of the bottom plate heater of the cell to minimize heat leakage. The maximum heat leakage was tested and found to be less than 0.5 W at highest temperature difference attained in this experiment. Figure 5 shows the Nusselt number as a function of Rayleigh number. The best fit gives $Nu \sim 0.20Ra^{0.25}$ which is slightly higher from He.

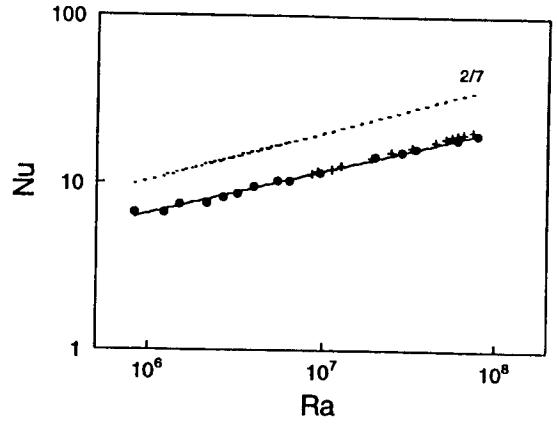

Figure 5. Scaling of Nusselt number as a function of Ra. The solid line is the slope (1/4).

Measurement of Boundary Layers

We measured the thermal boundary layer and the viscous boundary layer directly, using a thermistor suspended by a thin frame and moved vertically along the center line of the cylindrical cell by a stepper motor. Figure 6 shows probability distribution function (pdf) of temperature fluctuations at various heights along the center line of the cylinder. When the thermistor is well within the two boundary layers, the pdf is close to Gaussian, and approaches to an Exponential like distribution as the detector moves toward the center.

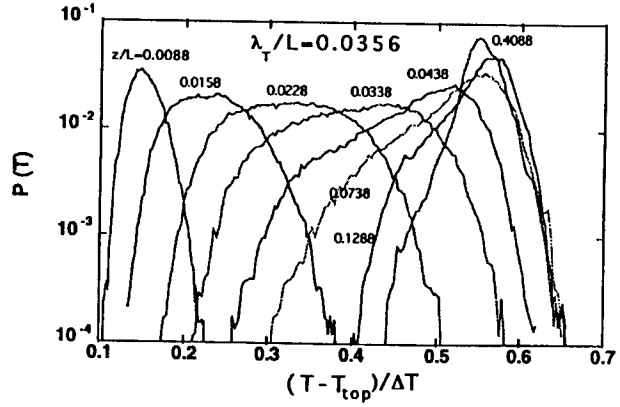

Figure 6. Probability distribution function of temperature fluctuation at various heights, z/L.

We plot the time average of the temperature, T, as a function of the distance from the top plate z in Figure 7(a). Temperature profiles fit the function $T_{ave}(z) - T_{top} = m_1 \tanh(m_2 z)$, which satisfies the requirement of linearity near to and saturation far from the boundary. We define the thermal boundary layer thickness as $\lambda_T = 1/m_2$ from the fit. Thus λ_T is the distance at which the extrapolation of the linear part of the profile equals the central mean temperature. The estimated thickness also agrees with the distance at which the root mean square of the temperature fluctuations, T_{rms}, reaches its maximum, as shown in Figure 7(a). We find $\lambda_T = 3.4$ mm at $Ra = 8.0 \times 10^7$.

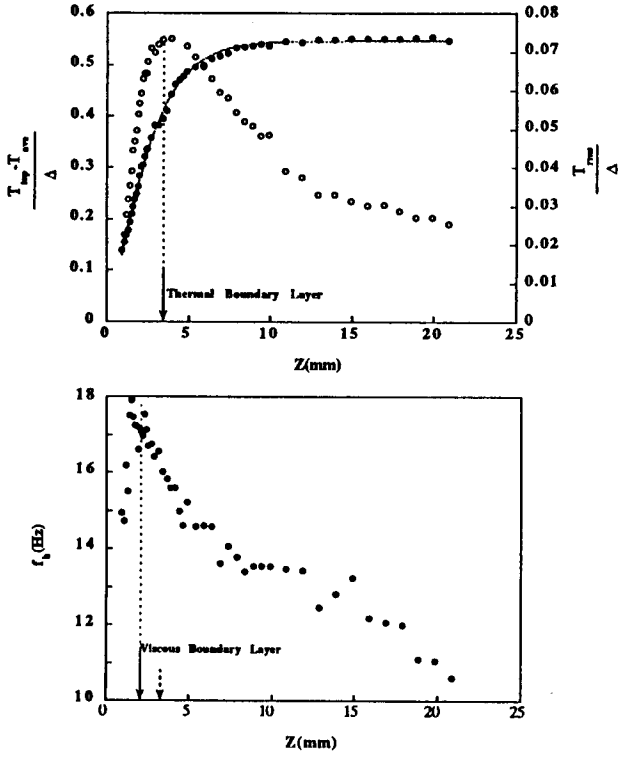

Figure 7. (a) Temperature profile (dots) and root mean square fluctuation (circles) near the top plate, measured by the movable thermistor [C]. The solid line is the best fit function, $T_{ave}(z) - T_{top} = m_1 \tanh(m_2 z)$. The guide line shows the thermal boundary layer thickness. (b) The profile of the frequency, f_h, as a function of the distance, z, from the top plate. The distance at which f_h reaches its maximum approximates the viscous boundary layer thickness.

We estimated the profile of the viscous boundary layer from the highest frequency, fh, of the temperature frequency spectrum. Measurements in water

and SF_6 [10, 15] have validated this method. In Figure 7 (b), we show f_h as a function of the distance z. As the viscous boundary layer thickness we took the distance at which f_h is maximal, to obtain $\lambda_\nu = 1.6$ mm at $Ra = 8.0 \times 10^7$, so $\lambda_\nu \sim 0.5\, \lambda_T$. This ratio differs in pressurized SF_6 for which λ_ν is much larger than λ_T (for instance $\lambda_\nu \sim 3\, \lambda_T$). Evidently the two boundary layers have crossed at this Ra. The length scale of two boundary layers at various Rayleigh number are shown in Figure 8. Two boundary layers are crossed in the whole range of Ra we measured. The solid line in Figure 8 shows the slope -0.25 for comparison.

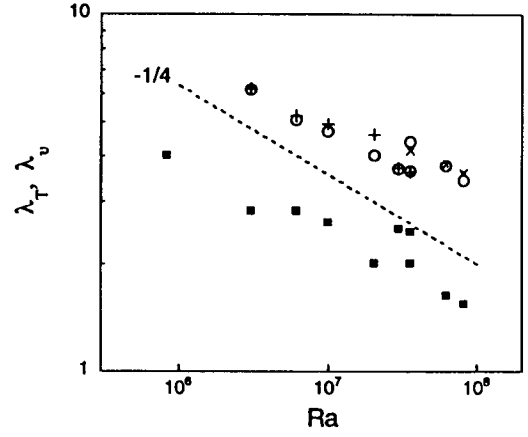

Figure 8. Thickness of thermal and viscous boundary layers as a function of Ra. Thermal boundary layer length is determined by the fitting of average temperature profile (○), and by the maximum position of the rms fluctuations (+). Viscous sublayer length is determined from the cutoff frequency f_h of power spectrum (square).

Discussion

We can estimate the Reynolds number of the shear flow based on boundary layer thickness, λ_ν, defined as,

$$Re_\lambda = \frac{U l_\nu}{\nu} . \qquad (7)$$

By using the mean flow scaling, $U\,L/\nu \sim 6.24 Ra^{0.46}$ and the data for λ_ν, we plot Re_λ as a function of Ra in Figure 9. Note that $Re_\lambda \sim 500$ at Ra $\sim 7 \times 10^7$, so the boundary layer is turbulent. Considering that the turbulent viscous boundary layer is as thin as or thinner than the thermal boundary layer, the plumes are stretched and mixed by the turbulent shear as soon as they detach from the

thermal boundary layer and before they arrive at the center of the fluid. Therefore simple plumes may not exist in low Prandtl number fluids.

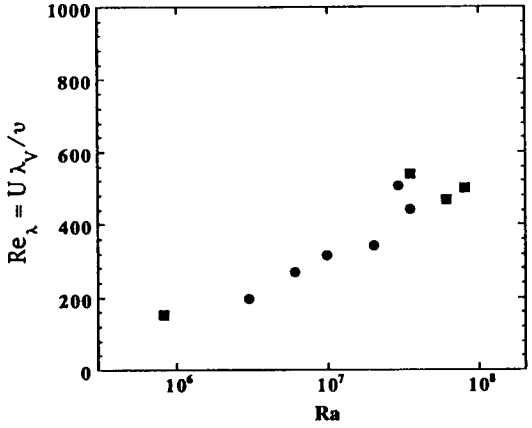

Figure 9. Reynolds number of the viscous sublayer, $Re\lambda_V = U\lambda_V/\nu$.

Additionally, the surface (boundaries and side walls) and bulk flows lie in different regimes. The typical temperature fluctuations (rms) at the center, θ, is about 3% of the total temperature difference, ΔT; thus $\theta/\Delta T \sim 10^{-2}$ at $Ra = 10^7$. The typical velocity is about 2 cm/sec at $Ra \sim 10^7$. The buoyancy force, $\alpha g\theta$, of the fluctuation at the center is much smaller than the inertial term, $\wedge | U \nabla U | \wedge \sim U^2/L$; $\alpha g\theta/(U^2/L) \sim 10^{-2}$, where α is the thermal expansion coefficient and g is the gravitational acceleration. Therefore, in the center region, buoyancy is negligible and temperature fluctuations resemble a passive scalar, perhaps causing the scaling behavior of the spectrum. We obtain a correct estimate (2 cm/sec) of the mean flow velocity by balancing the buoyancy of the boundary layer, $\alpha g\Delta T$, with the inertial term, U^2/L; implying that most of the detached boundary layer flows along the side wall in the large scale circulation, which drives the turbulent flow in the center.

At larger scales, inertia balances the buoyancy term, while at smaller scales inertia balances the energy transfer. The Bolgiano scale, L_B, at which buoyancy and energy transfer are of the same order, is given by $L_B = Nu^{1/2}L/(Ra \cdot Pr)^{1/4}$. [18] In the experiment $L_B \sim 2$ cm at $Ra = 10^7$, which corresponds to 1 Hz in the spectrum, narrowing the cascade range.

We did not observe a transition to $Nu \sim Ra^{1/2}$. Further experimental study of higher Ra number flow is in progress.

Summary

In thermal turbulence in low Prandtl number fluids like Hg, due to the small kinematic viscosity, the turbulent state is well developed over the observed range of Ra ($10^6 < Ra < 10^8$) as shown by the histogram of temperature fluctuations and Reynolds number. Scaling exponents of Nu is slightly smaller than that of He. The scaling of the cutoff frequency, f_c, of the temperature frequency spectrum is peculiar and results in narrowing of the cascade range. Measurement of the boundary layer profile shows that the viscous and thermal boundary layers have crossed. The detachments from the boundary layers are strongly affected by the turbulent shear flow. This phenomena, combined with large scale circulation causes the turbulent flow in the center part to be driven by shear. The temperature fluctuations in the center behave as a passive scalar resulting the peculiar scaling of the power spectrum. A transition to $Nu \sim Ra^{1/2}$ was not observed.

References

1 F. Heslot, B. Castaing and A. Libchaber, Phys. Rev. A **36**, 5870 (1987).
2 B. Castaing et al., J. Fluid Mech. **204**, 1 (1989).
3 M. Sano, X. Z. Wu and A. Libchaber, Phys. Rev. A, **40**, 6421 (1989), X. Z. Wu and A. Libchaber, Phys. Rev. A, **45**, 842 (1992).
4 X. Z. Wu, L. P. Kadanoff, A. Libchaber and M. Sano, Phys. Rev. Lett. **64**, 2140 (1990).
5 T. H. Solomon and J. P. Gollub, Phys. Rev. Lett. **64**, 2382 (1990); Phys. Rev. A **43**, 6683 (1991).
6 W. V. R. Malkus, Proc. R. Soc. London A **225,** 185, (1954); L. N. Howard, J. Fluid Mech. **17,** 405, (1963).
7 B. I. Shraiman and E. D. Siggia, Phys. Rev. A **42**, 3650 (1990).
8 R. Kraichnan, Phys. Fluids, **5,** 1374, (1962).
9 T. Takeshita, T. Segawa, J. A. Glazier and M. Sano, Phys. Rev. Lett., **76,** 1465 (1996).
10 A. Belmonte, A. Tilgner and A. Libchaber, Phys. Rev. Lett. **47**, 4067 (1993); Phys. Rev. E **50**, 269 (1994).
11 R. Bolgiano Jr., J. Geophys. Res. **64,** 2226, (1962); 3023, (1962).
12 A. M. Obukhov, Dokl. Akad. Nauk. SSSR, **121,** 1246, (1959) [Sov. Phys. Dokl. **3,** 61, (1959).]
13 A. Brandenburg, Phys. Rev. Lett., **69,** 605, (1992); V. Yakhot, Phys. Rev. Lett., **69,** 769, (1992); S. Toh and E. Suzuki, Phys. Rev. Lett. **73,** 1501, (1994).
14 X. Z. Wu, Ph. D Thesis, the University of Chicago (1991).
15 A. Tilgner, A. Belmonte, and A. Libchaber, Phys. Rev. E **47**, 2153, (1993).
16 S. Globe and D. Dropkin, J. Heat Transfer 24, (1959).
17 S. Cioni, S. Ciliberto and J. Sommeria, in Dynamics of Atmospheres and Oceans special issue (October, 1995).
18 R. Benzi, R. Tripiccione, F. Massaioli, S. Succi and S. Ciliberto, Europhys. Lett. **25,** 341, (1994); S. Cioni, S. Ciliberto and J. Sommeria, to appear in Europhys. Lett. (1995).